An Adaptive Sparse Constraint ISAR High Resolution Imaging Algorithm Based on Mixed Norm

Daiyue SONG, Qianqian CHEN, Kaizhuang LI

The College of Electronic and Information, Qingdao University, Qingdao, Shandong, China

898176542@qq.com, qqchen@qdu.edu.cn, 1397089192@qq.com

Submitted April 20, 2022 / Accepted September 14, 2022 / Online first October 7, 2022

Abstract. *Based on the sparsity of inverse synthetic aperture radar (ISAR) signal, in this paper, a novel high resolution imaging algorithm is proposed. In this method, an optimal ISAR signal model based on mixed norm is established by using compressed sensing theory. The high-resolution ISAR image with short coherent accumulation time is realized by solving the optimization model. The main advantages of the proposed approach are: The model makes use of the $l_{2,0}$ mixed norm to realize faster convergence and improve the computational speed of the model solution obviously. Moreover, according to the result sparsity of each iteration under arbitrary noise, the regularization coefficient in the model can be adjusted adaptively, which avoids the complex process of repeated attempts, otherwise, the optimal coefficient needs to be estimated and attempted by the statistical characteristics of the noise and signal. The effectiveness of the proposed method is verified by simulated and measured data.*

Keywords

Inverse Synthetic Aperture Radar (ISAR), mixed norm, regularization coefficient, sparse constraint

1. Introduction

The imaging process of inverse synthetic aperture radar (ISAR) is a two-dimensional high-resolution imaging process, which static radar conducts range and azimuth imaging of moving targets [1]. In conventional ISAR process, like Range-Doppler (RD) algorithm, in order to obtain high-resolution ISAR image, the target echo data is obtained by the radar first. Then, the range high resolution imaging is achieved by sending large bandwidth signals and azimuth imaging high resolution achieved by long coherent processing interval (CPI) accumulation. Next, motion compensation needs to be implemented (including range-alignment and initial phase-adjustment). Finally, the coherent accumulation of range and azimuth are realized by Fourier transform. However, in practical application, ISAR targets are non-cooperative and mobile generally, so it is difficult to ensure the smooth movement of targets during long CPI observation. The data of long CPI will increase the complexity of imaging processing and consume more storage space.

In contrast, short CPI observation of the target is more conducive to subsequent real-time imaging and recognition. In short CPI observation, the target movement is closer to stable and the scattering characteristics of the target are relatively stable. In addition, more 2-dimensional ISAR image sequences can be obtained by ISAR imaging of short CPI under the condition of the same data length, which is very beneficial to imaging calibration [2]. However, in short CPI observation, the echo number of signal is much smaller than that of full aperture, and part of the echo data is missing, which obviously affects the Fourier transform process. At this time, the imaging result obtained by RD algorithm have low resolution, and the distribution characteristics and structure characteristics of target scattering points cannot be accurately presented, which is not conducive to target identification and other subsequent operations. ISAR imaging has a feature that the strong scattering center of the target occupies only a few pixel points in the whole imaging plane, and most of the energy of the scattering field is only contributed by a few strong scattering points, which indicates that ISAR images have strong sparsity [3]. Full-aperture high-resolution ISAR images under short CPI observation can be effectively achieved by the existing compressed sensing theory (CS) [4] based on sparsity of images [5].

In view of the above theory, many high-resolution imaging algorithms based on CS have been proposed. In fact, the purpose of the algorithm is to achieve the high-resolution reconstruction of target signal, that is, the target information is recovered accurately by the short CPI observation signal in the presence of noise interference. The super-resolution imaging algorithm based on ordinary CS is proposed [6], which can accurately recover an unknown sparse signal from low-dimensional observation data to high-dimensional detailed data by solving a minimal-norm constrained optimization problem. But the signal and noise are treated equally in the CS imaging method, so it cannot perform well under the condition of low Signal to Noise Ratio (SNR). To solve this problem, an algorithm based on weighted compressed sensing (WCS) is proposed [7]. In the algorithm, signal and noise are distinguished by

DOI: 10.13164/re.2022.0477

weights in different environments, so it has better noise tolerance performance to improve the imaging algorithm under low SNR image. Although CS and WCS algorithms have achieved high-resolution image imaging in the case of short CPI, as these two algorithms need to be optimized and solved by CVX method, they have great challenges in terms of operation complexity and efficiency. Therefore, an improved smoothed l_0 norm sparse signal reconstruction ISAR imaging algorithm is proposed [8], which has good results in operation speed and imaging accuracy. However, many parameters in it require constant debugging to find the best value, so the influence of human factors on imaging results needs to be improved. With the in-depth research, a high-resolution imaging algorithm based on l_1 norm sparse constraint is proposed, which combines the conjugate gradient algorithm to ensure the imaging accuracy [9]. In this algorithm, a method is derived to recover the target image accurately through the observation sample information, noise and target statistics information. However, the speed of the algorithm needs to be improved. Another, the sparsity of the sampled signal and noise used to estimate the regularization coefficient is not obvious enough, so the regularization coefficient determination process is cumbersome. In order to improve the efficiency, combing the relation between regularization coefficient and signal sparsity [10], we propose an adaptive sparse constraint ISAR high resolution Imaging algorithm based on $l_{2,0}$ mixed norm. The main advantages of the proposed algorithm are

1) In this algorithm, a sparse constrained optimization model is established by using the $l_{2,0}$ mixed norm. The $l_{2,0}$ mixed norm combines the advantages of l_2 norm and l_0 norm [11], which optimizes the convergence of the model and improves the computing speed of the model solution.

2) The regularization coefficient in the model of this algorithm can be adjusted adaptively according to the result sparsity of each iteration, and the relatively stable coefficient can be determined during only a few iteration cycles. This method avoids the complex process of repeated attempts because the optimal coefficient needs to be estimated by the statistical characteristics of the noise and signal, so that improves the efficiency of the algorithm.

3) Fast Fourier Transform (FFT) and conjugate gradient descent are used in the iterative operation of this algorithm model, which simplifies the operation complexity and improves the solving efficiency.

The paper is organized as follows. Section 2 proposes the rotating signal model and the basis of optimization signal model of ISAR imaging is briefly introduced based on previous works. In Sec. 3, the optimization model is proposed and the solution algorithm is given to reconstruct the target signal by authors. ISAR imaging results of simulated and measured data are presented in Sec. 4. Finally, Section 5 provides the conclusion and possible future directions.

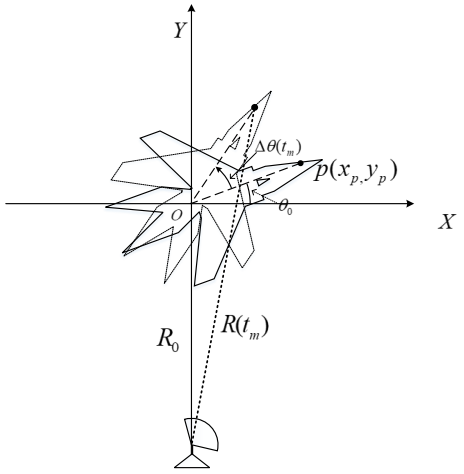

Fig. 1. Rotation signal model.

2. ISAR Imaging Signal Model

It is assumed that the range-alignment and initial phase-adjustment have been achieved [12], and then the rotation signal of the target model obtained is shown in Fig. 1.

In the case of short CPI observation, the angle change of the target relative to the radar can be approximated as

$$\Delta\theta(t_m) \approx \omega t_m \tag{1}$$

where t_m is slow time, T represents coherent processing time length, and $0 \le t_\mathrm{m} \le T$; ω is the rotational angular velocity of the target. while the distance between the target and the radar is much larger than the size of the reflected target, the whole process of radar transmitting and receiving signal can be approximated to the plane where the radar and the target are connected. At this time, the distance from the scattering point $p(x,y)$ on the target to the radar can be expressed as

$$r(t_\mathrm{m}) = r_0 + y\cos\left(\Delta\theta(t_\mathrm{m})\right) + x\sin\left(\Delta\theta(t_\mathrm{m})\right) \tag{2}$$

where r_0 is the distance between radar and target rotation center O. In short CPI observation, the target rotation angle $\Delta\theta(t_\mathrm{m})$ is so small that can be replaced by (1), and the approximate formula of the distance between target scattering point and radar can be obtained

$$r(t_\mathrm{m}) = r_0 + y + x\sin\left(\omega t_\mathrm{m}\right). \tag{3}$$

In general, the radar transmitting signal is linear frequency modulation signal $s(t_\mathrm{r})$

$$s(t_\mathrm{r}) = \mathrm{rect}\left[\frac{t_\mathrm{r}}{T_\mathrm{p}}\right]\cdot\exp\left[2\pi\mathrm{j}(f_\mathrm{c}t_\mathrm{r} + \frac{\alpha}{2}t_\mathrm{r}^{\,2})\right] \tag{4}$$

where t_r represents fast time; T_p is pulse width; f_c is the carrier frequency; α is the modulation frequency; rect[.] represents a window function. The Migration Though Resolution Cell (MTRC) may appear in the target movement

when its size is large, which can be compensated by some way [13]. The echo signal after compensated and pulse compressed is obtain as

$$s(t_r,t_m)\approx b_p\cdot\mathrm{rect}\left[\frac{t_\mathrm{m}}{T}\right]\cdot\sin c\left[T_\mathrm{p}\alpha\left(t_\mathrm{r}-\frac{2(r_0+y)}{C}\right)\right]\cdot\exp\left[-\mathrm{j}4\pi\frac{r(t_\mathrm{m})}{\gamma}\right] \tag{5}$$

where b_p is the scattering coefficient of the target, which can be regarded as a constant when the rotation angle of the target is small; γ is the radar transmitting signal wavelength; C is the transmission speed of electromagnetic wave. In the case of considering noise, when there are N scattering points in the range cell with a distance of $r_0 + y$, the echo signal of this range cell is expressed as

$$s(t_\mathrm{m})=\sum_{p=1}^{N}B_p\cdot\mathrm{rect}\left[\frac{t_m}{T}\right]\cdot\exp(-2\pi\mathrm{j}f_pt_\mathrm{m})+n \tag{6}$$

where B_p is the scattering coefficient of the scattering point p; f_p is the Doppler frequency of the scattering point, n is additive noise.

And, $B_p=b_p\cdot\exp(-4\pi\mathrm{j}\frac{r_0+y}{\gamma})$; $f_p=\frac{2\omega x}{\gamma}$.

The pixel distribution of the image domain can be obtained by making the azimuth Fourier transform of (6)

$$s(f_\mathrm{d})=\sum_{p=1}^{N}B_p\cdot\sin c[T(f_\mathrm{d}-f_p)]+n\cdot \tag{7}$$

3. ISAR Super-Resolution Imaging Based on Mixed Norm Sparse Constraint

3.1 Optimization Imaging Model Based on Mixed Norm Sparse Constraint

When the target is observed with short CPI, it can be assumed that the target is moving smoothly and the signal echo is more stable. The signal model shown in (6) can be discretized based on the sparse characteristics of ISAR signal. If there are $\bar{M}$ effective pulses in each range cell under short CPI observation, ISAR echo signal at this time is expressed as

$$\mathbf{S}=\mathbf{FX}+\mathbf{n} \tag{8}$$

where $\mathbf{S}$ is the short CPI observation matrix of size $\bar{M}\times N$, $\bar{M}$ is the total number of sampling pulses, N represents the sampling points of range profile; $\mathbf{X}$ is the observation target to be reconstructed of size $M\times N$, and M is the number of pulses emitted by signals under full-aperture observation; $\mathbf{n}$ represents additive noise matrix; $\mathbf{F}$ represents the partial Fourier transform matrix of size $\bar{M}\times M$, and $\bar{M}<M$.

And, $\mathbf{F}=\begin{pmatrix}1 & 1 & \cdots & 1\\ 1 & \omega & \cdots & \omega^{M-1}\\ \vdots & \vdots & \ddots & \vdots\\ 1 & \omega^{\bar{M}-1} & \cdots & \omega^{(\bar{M}-1)(M-1)}\end{pmatrix}_{\bar{M}\times M}$ where,

$\omega=\exp\left(-\mathrm{j}\frac{2\pi}{M}\right)$.

The solution of the matrix $\mathbf{X}$ is to recover the target signal accurately in the presence of noise interference. In this section, ISAR high-resolution imaging algorithm in short CPI will be derived by using the statistical characteristics of the observation samples, noise and target.

In (8), all elements in noise $\mathbf{n}$ obey the complex Gaussian random distribution with mean value of zero and standard deviation of σ, and the elements are independent of each other. The sparsity of target signals usually obeys the Laplace probability distribution, and the Laplace scale coefficient is η. According to the Bayesian compressed sensing theory [14], the maximum posterior probability (MAP) estimation expression of target signal $\mathbf{X}$ is

$$\hat{\mathbf{X}}=\arg\min\left\{\left\|\mathbf{S}-\mathbf{FX}\right\|_2^2+\lambda\left\|\mathbf{X}\right\|_1\right\} \tag{9}$$

where $\lambda=2\sigma^2\eta$ represents the constraint coefficient of l_1 norm. In the case of uncertain SNR, λ is adjusted according to the fidelity and noise suppression degree of effective signal to balance the relationship between image sparsity and estimation error [15]. The solution of (9) is regarded as a l_1 norm regularization problem [16].

However, in this optimization model, the convergence of l_1 norm is not very well, which will affect the convergence speed of the solution process. In addition, lambda needs to be estimated according to the statistical characteristics of noise and signal, which seriously affects the efficiency and accuracy of model solving. Therefore, a new ISAR high-resolution imaging model is obtained combining the $l_{2,0}$ mixed norm, which expression is shown as

$$\hat{\mathbf{X}}=\arg\min\left\{\left\|\mathbf{S}-\mathbf{FX}\right\|_2^2+\lambda\left\|\mathbf{X}\right\|_{2,0}\right\} \tag{10}$$

where, the $\|\mathbf{X}\|_{2,0}$ mixed norm is defined as first taking the l_2 norm of the row vector of the matrix $\mathbf{X}$ to get a column vector, then taking the l_0 norm of the column vector to get the $l_{2,0}$ mixed norm of the matrix $\mathbf{X}$. The $l_{2,0}$ mixed norm has a better convergence speed because it combines the advantages of l_2 norm and l_0 norm (the l_2 norm divides the signal into clusters, while the l_0 norm makes use of the sparsity of the signal) [10].

However, considering that $l_0$norm minimization is a non-polynomial (NP) problem in practice, the norm is usually approximated by a continuous function [17]. A commonly used approximate expression is shown as

$$\left\|\mathbf{X}_{\boldsymbol{n}}\right\|_0 = \sum_{m=1}^{M}\left(1-\exp(-\beta\left|x_{mn}\right|)\right) \tag{11}$$

where $\beta < 0$, so the $l_{2,0}$ mixed norm approximation formula is

$$\left\|\mathbf{X}\right\|_{2,0} = \sum_{m=1}^{M}\left(1-\exp(-\beta\left\|\mathbf{X}_{\boldsymbol{m}}\right\|_2)\right). \tag{12}$$

Thus, the expression of ISAR high-resolution imaging model based on sparse constraints of $l_{2,0}$ mixed norm can be shown as

$$\hat{\mathbf{X}} = \arg\min\left\{\left\|\mathbf{S}-\mathbf{F}\mathbf{X}\right\|_2^2 + \lambda\sum_{m=1}^{M}\left(1-\exp(-\beta\left\|\mathbf{X}_{\boldsymbol{m}}\right\|_2)\right)\right\}. \tag{13}$$

Although Equation (13) can complete the accurate recovery of the target image $\mathbf{X}$. It can be seen from the extraction process above that the determination of the constraint coefficient λ needs to be adjusted according to the noise variance σ and the Laplace coefficient η. So the steps to get the optimal coefficient is cumbersome.

In fact, the reconstruction accuracy and sparsity of the solution is influenced by regularization coefficient λ in (13) [18]. When the optimization is solved in each iteration, the sparsity representation of the signal will be more obvious, so each iteration will be more conducive to obtaining high-resolution image when regularization coefficient of the model can update adaptively. And then, an adaptive expression of regularization coefficient λ adapted to the above model can be obtained by combining regularization theory [19] as

$$\lambda^{n+1} = \left|\mathbf{X}^n\right|_{k+1} / u \tag{14}$$

where k is the sparsity of the signal. $|\mathbf{X}|_k$ is the modulus of the first k component of $\mathbf{X}$. The convergence of the iterative process is controlled by u and

$$0 < u^{-1} < \left\|\mathbf{F}\right\|_2^2. \tag{15}$$

3.2 Solution of ISAR Optimal Imaging Model

The quasi-Newton algorithm [20] is adopted to solve the optimization problem shown in (13). In order to avoid the undifferentiable problem in the process of solving the mixed norm, a minimal non-negative value δ is used to approximate (13)

$$\begin{aligned}\hat{\mathbf{X}} = &\\ \arg\min&\left\{\left\|\mathbf{S}-\mathbf{F}\mathbf{X}\right\|_2^2 + \lambda\sum_{m=1}^{M}\left(1-\exp(-\beta\sqrt{\sum_{n=1}^{N}\left|x_{mn}\right|^2+\delta})\right)\right\}\\ &= \arg\min\left(f(\mathbf{X})\right),\end{aligned} \tag{16}$$

the conjugate gradient of $f(\mathbf{X})$ is

$$\begin{aligned}\nabla f(\mathbf{X}) &= 2\mathbf{F}^{\mathrm{H}}\mathbf{F}\mathbf{X} + \lambda\Lambda(\mathbf{X})\mathbf{X} - 2\mathbf{F}^{\mathrm{H}}\mathbf{S}\\ &= H(\mathbf{X})\mathbf{X} - 2\mathbf{F}^{\mathrm{H}}\mathbf{S}.\end{aligned} \tag{17}$$

Among (15), the Hessian matrix is

$$H(\mathbf{X}) = 2\mathbf{F}^{\mathrm{H}}\mathbf{F} + \lambda\Lambda(\mathbf{X}) \tag{18}$$

where $\Lambda(\mathbf{X})$ is a diagonal matrix

$$\Lambda(\mathbf{X}) = \left(\mathrm{diag}\left[\beta\frac{\exp\left(-\beta\sqrt{\left|\mathbf{X}_{\boldsymbol{m}}\right|^2+\delta}\right)}{\sqrt{\left|\mathbf{X}_{\boldsymbol{m}}\right|^2+\delta}}\right]\right)_{m\times m}. \tag{19}$$

Because the Hessian matrix contains the objective function to be solved, it can be solved directly by iterative method

$$\hat{\mathbf{X}}^{n+1} = \left[H(\hat{\mathbf{X}}^n)\right]^{-1}\mathbf{F}^{\mathrm{H}}\mathbf{S}_{\boldsymbol{k}} \tag{20}$$

where $[.]^{-1}$ represents the inverse of the matrix; $\hat{\mathbf{X}}^n$ represents the result of the first n iteration of the objective function $\mathbf{X}$; λ in $H(\mathbf{X})$ is updated with each iteration. The convergence threshold ρ is set, and when the convergence condition of the objective function meets $\left\|\hat{\mathbf{X}}^{n+1}-\hat{\mathbf{X}}^n\right\|_2^2 \Big/ \left\|\hat{\mathbf{X}}^n\right\|_2^2 \le \rho$, the iteration cycle ends and the objective result is obtained.

It is worth discussing an important feature of (20), that is, the major computational load is from the calculation of matrix inversion and Fourier matrix product in the algorithm. To avoid the inverse processing, we use the conjugate gradient algorithm and FFT operations for the solution [21]. Compared with the traditional Cholesky [22] operation, this algorithm has an order of magnitude improvement in operation efficiency.

4. Experiments and Analyses

In this part, simulated data and measured data are used to verify the operation effect of the algorithm. During the verification process, the algorithm proposed in this paper is compared with the improved imaging algorithm based on l_1 norm. The above two algorithms are used to calculate the data under different noise, and the results are compared. In order to verify the reconstruction performance of the algorithm, the paper tests the algorithm through the MATLAB 2020a processing platform and run on a working station with AMD Ryzen 7 4800H CPU at 2.90 GHz and 16.0 GB RAM.

4.1 Simulated-Data Experiments

In the simulation experiment, the aircraft model used is $70 \times 60 \times 9$ m^3, consisting of 330 scattered points. The aircraft point target model used in the experiment is shown in Fig. 2.

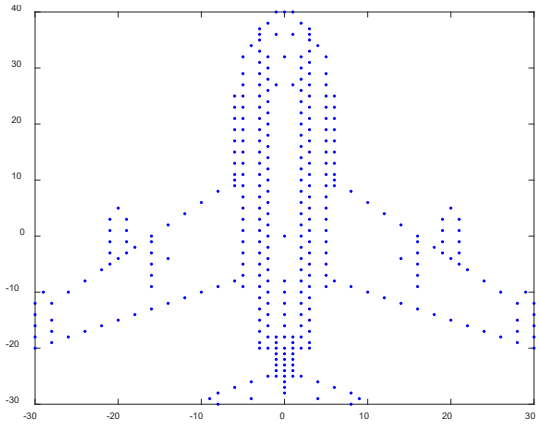

Fig. 2. The aircraft point target model.

The radar carrier frequency is 9.6 GHz, the radial velocity is 100 m/s, the radial acceleration is 5 m/s^2, the pulse repetition frequency is 100 Hz, the rotational angular velocity is 0.5 °/s, and the range direction resolution is 0.375 m.

In the simulation, the pulse compression is carried out by dechirp. The distance between the radar and the target rotation center is 10000 m, and the amplitude of each scattering point is 1. Under the short CPI observation, 64 echo pulse is generally used as the standard, and the super-resolution image with 256 pulses length is reconstructed for comparison.

Figure 3 and Figure 4 are the calculation results of testing the simulated data without noise. The range profile produced by 64 echo pulses after translation compensation is shown in Fig. 3. The imaging result of RD algorithm is shown in Fig. 4. It can be seen that the traditional ISAR imaging algorithm cannot accurately focus the short CPI data, and a high-resolution imaging algorithm should be adopted.

In order to show the difference between before and after the algorithm is improved, the two high resolution imaging algorithms mentioned in this paper were used to solve the problem. The parameters are set as follows: the threshold of iteration is $\rho = 10^{-4}$, the upper limit of iteration is 500, parameter $\beta = 20$, and the constant is $\delta = 10^{-6}$.

The result based on l_1 norm sparse constraint high resolution imaging algorithm is shown in Fig. 5. The result of algorithm proposed in this paper is shown in Fig. 6. The number of iterations of the algorithm based on the l_1 norm reached the upper limit of 500, but do not reach the set threshold of iteration termination ρ, which takes 326.8044 s. The algorithm proposed in this paper iterates for 7 times and get basically stable $\lambda = 0.0011$. It iterates for 245 times and reaches the iteration termination, which takes 149.7694 s. It can be seen that the imaging efficiency of the algorithm proposed in this paper is higher than that of the l_1 norm and the regularization coefficient λ can be obtained adaptively after a few iterations.

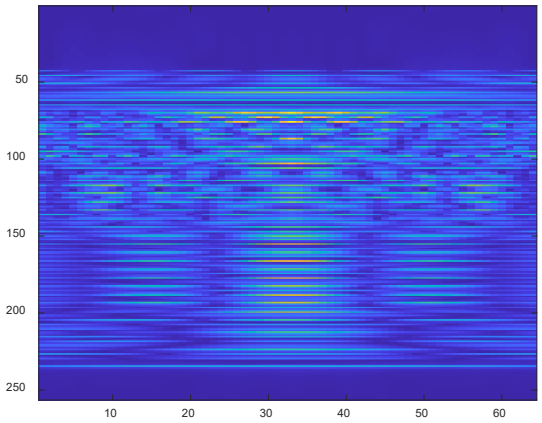

Fig. 3. Range profile of simulated data.

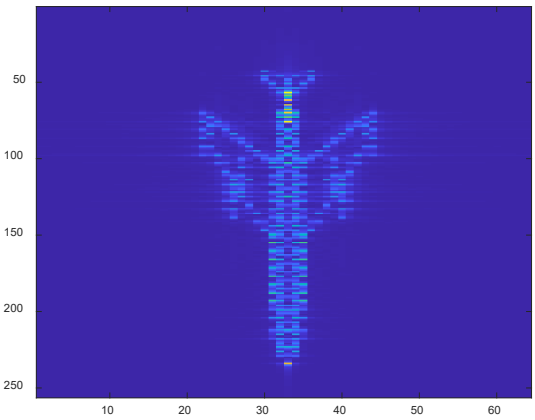

Fig. 4. Imaging result of RD algorithm.

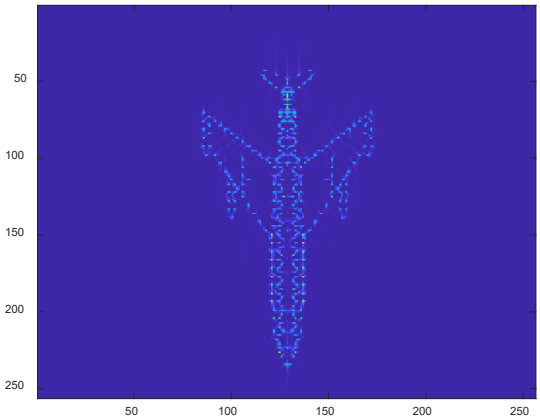

Fig. 5. Imaging result of L1 norm.

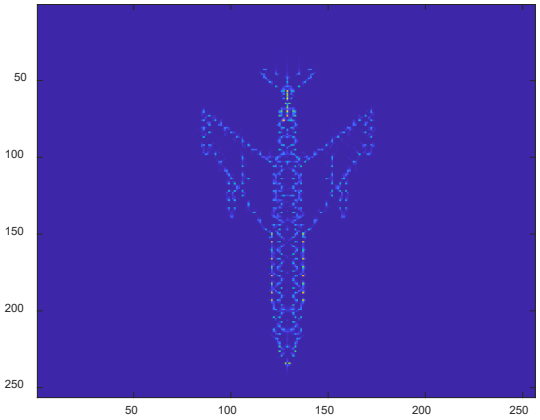

Fig. 6. Imaging result of the algorithm proposed in this paper.

In order to further reflect the advantages of the algorithm, the results of two high resolution imaging algorithms under small amount of echo pulses are compared. Under the short CPI observation, through 50 experiments with numbers of echo pulses ranging from 32 to 64 in step of 4, and the super-resolution image with the length of 256 is reconstructed.

Taking 48 echo pulses as an example, the imaging results obtained by the two algorithms are shown in Fig. 7 and Fig. 8 respectively. The algorithm based on the l_1 norm iterates upper limit times, but does not reach the set threshold of iteration termination ρ, which takes 390.7043 s. The algorithm proposed in this paper iterates for 13 times and get basically stable $\lambda = 0.0021$. It iterates for 261 times and reaches the iteration termination, which takes 156.5628 s. It can be seen that the imaging efficiency of the algorithm proposed in this paper is higher than that of the l_1 norm under small amount of echoes.

Under different number of echo pulses, two high-resolution imaging algorithms are used for operation. The average operation time comparison results of 50 repeated experiments are shown in Fig. 9. In the figure, the black broken line is the running time required by the original algorithm, while the red broken line is the running time required by the algorithm proposed in this paper.

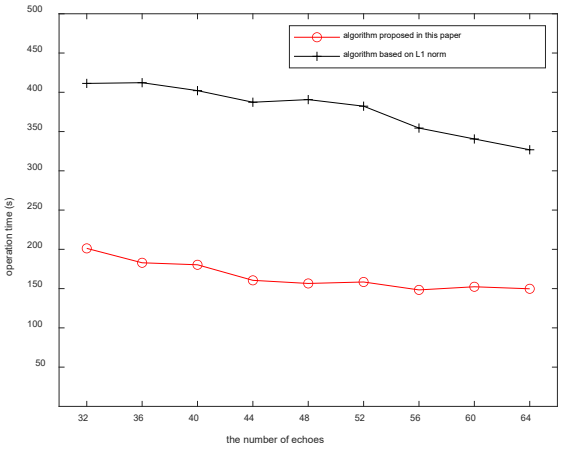

Fig. 9. Curve of operation time with the number of echo pulses.

It can be seen that the operation time of the algorithm based on the mixed norm proposed in this paper is smaller than the previous algorithm at different numbers of echoes.

In order to more accurately reflect the advantages of the algorithm in the natural environment, in the case of adding white Gaussian noise, the two algorithms are tested and compared through 50 experiments with SNR ranging from 4 dB to 20 dB in step of 2 dB.

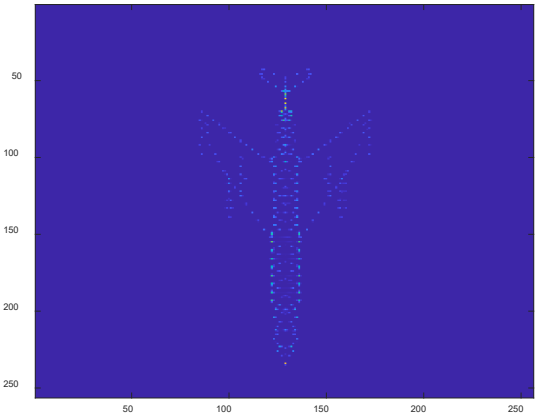

Fig. 7. Imaging result of L1 norm using 48 pulses.

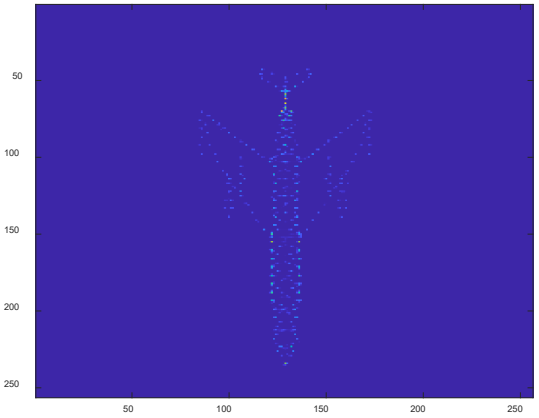

Fig. 8. Imaging result of the algorithm proposed in this paper using 48 pulses.

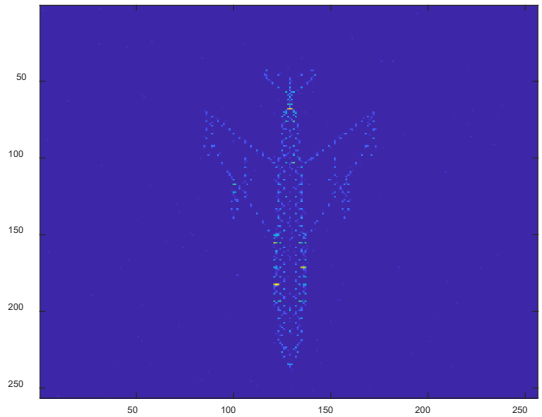

Fig. 10. Imaging result of L1 norm at SNR =5 dB.

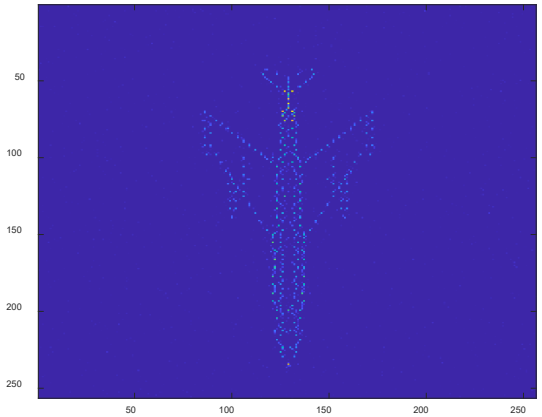

Fig. 11. Imaging result of the algorithm proposed in this paper at SNR=5 dB.

Taking the SNR of 5 dB as an example, under the short CPI observation, 64 echoes are taken for processing and the super-resolution image with the length of 256 is reconstructed. The imaging results obtained by the two algorithms are shown in Fig. 10 and Fig. 11 respectively. It can be seen that the algorithm proposed in this paper can still achieve relatively clear high-resolution imaging under the condition of low SNR. It can be proved by correlation coefficient and there is little difference between the two methods, which are 0.7851 in Fig. 10 and 0.7831 in Fig. 11. The correlation coefficient can be expressed as

$$C_{\text{coef}} = \left\langle \left|\bar{\mathbf{X}}\right| \cdot \left|\hat{\mathbf{X}}\right| \right\rangle \Big/ \left\|\bar{\mathbf{X}}\right\| \cdot \left\|\hat{\mathbf{X}}\right\| \tag{21}$$

where $\bar{\mathbf{X}}$ is the full aperture image reconstructed from all 256 echoes.

However, in Fig. 10, the number of iterations reaches the threshold of 500, which takes 326.1982 s. In Fig. 11, a stable $\lambda = 0.0045$ is obtained after 26 iterations, and the result is obtained after 131 iterations, which takes 209.5215 s. It can be seen that the imaging efficiency of algorithm proposed in this paper is higher than that of the l_1 norm in the case of noise.

Under different noises, two high-resolution imaging algorithms are used for operation. The average operation time comparison results of 50 repeated experiments are shown in Fig. 12.

In Fig. 12, the black broken line is the running time required by the original algorithm, while the red broken line is the running time required by the algorithm proposed in this paper. In general, the running time of the algorithm based on the mixed norm proposed in this paper is smaller than the previous algorithm under different SNRs.

In order to verify the effectiveness of the algorithm more comprehensively, the simulation results in the state of small amount of echo pulses and low SNR combined are presented.

The 48 echo pulses were used for simulation to compare at the SNR of 5 dB, the imaging results obtained by the two algorithms are shown in Fig. 13 and Fig. 14. It can

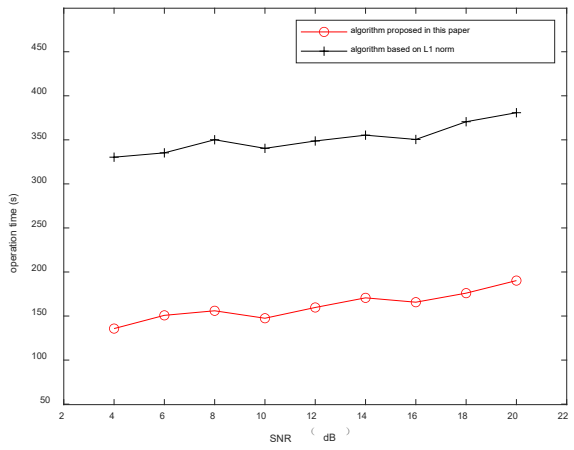

Fig. 12. Curve of operation time with SNR.

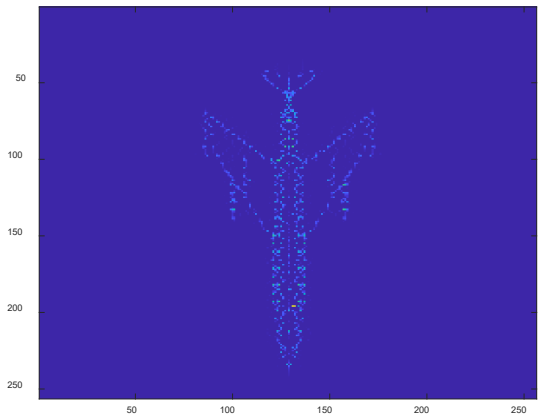

Fig. 13. Imaging result of L1 norm using 48 pulses at SNR = 5 dB.

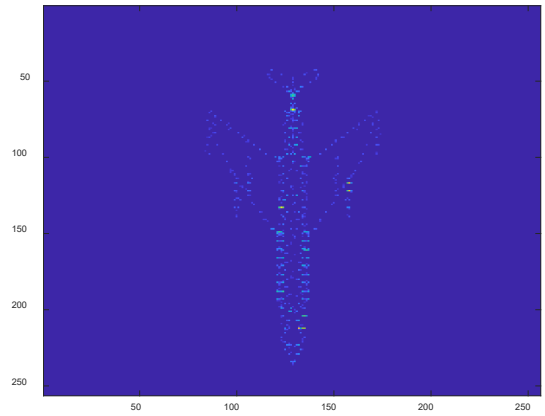

Fig. 14. Imaging result of the algorithm proposed in this paper using 48 pulses at SNR = 5 dB.

be proved by correlation coefficient which are carried out with 50 iterations and there is little difference between the two methods, which are 0.7764 in Fig. 13 and 0.7722 in Fig. 14.

However, in Fig. 13, the number of iterations reaches the upper limit of 500, which takes 356.2474 s. In Fig. 14, a stable $\lambda = 0.0052$ is obtained after 35 iterations, and the result is obtained after 178 iterations, which takes 198.7357 s. It can be seen that the imaging efficiency of the algorithm proposed in this paper is higher than that of the l_1 norm in this case.

4.2 Measured-Data Experiments

In order to further verify the advantages of the algorithm in this paper, the measured data of aircraft YAK-42 are used for processing. The carrier frequency of the radar is 9 GHz, the signal bandwidth is 400 MHz, the pulse repetition frequency is 100 Hz, the target velocity is 100 m/s, and the rotational angular velocity is 0.013 rad/s.

Figure 15 and Figure 16 are the calculation results of the measured data. The range profile produced by 64 echo pulses after translation compensation is shown in Fig. 15. The imaging result using conventional ISAR imaging algorithm is shown in Fig. 16. It also can be seen that the tradi-

tional ISAR imaging algorithm cannot accurately focus the measured data. In high-resolution imaging algorithm, parameter settings are the same as simulated data processing.

Figure 17 shows the running result of the high resolution imaging algorithm based on l_1 norm sparse constraints. The running result of the improved high-resolution imaging algorithm based on $l_{2,0}$ mixed norm obtained in this paper is shown in Fig. 18. When the measured data are used for testing, the number of iterations of the two algorithms both reached the upper limit of 500 times, which do not reach the

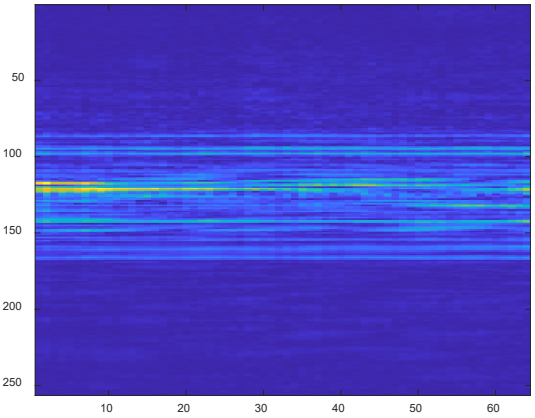

Fig. 15. Range profile of measured data.

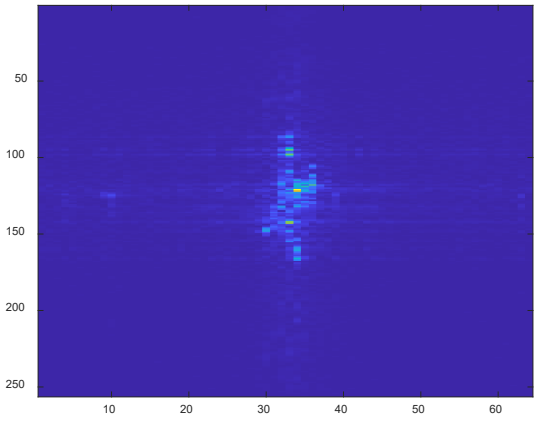

Fig. 16. Imaging result of RD algorithms.

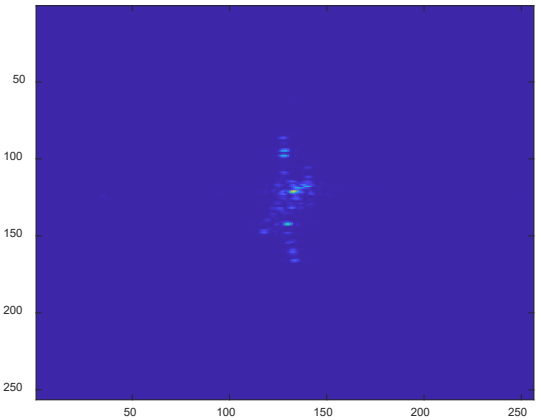

Fig. 17. Imaging result of L1 norm.

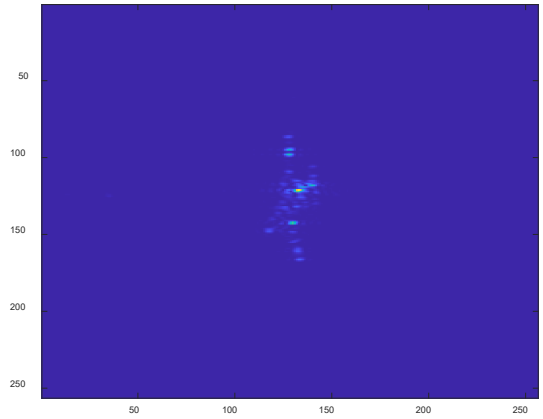

Fig. 18. Imaging result of the algorithm proposed in this paper.

set threshold of iteration termination ρ. However, due to the different convergence of the norms contained in the two algorithms, the convergence speed is still different to some extent. The operation time of algorithm based on l_1 norm is 542.6968 s, and the algorithm proposed in this paper takes 411.1321 s. It can be seen that the operation efficiency of the algorithm based on mixed norm is higher than that of the original algorithm under the measured data.

5. Conclusion

In this paper, based on the sparse characteristics of ISAR images, an optimization ISAR signal model based on mixed norm sparse constraints is proposed. The model takes advantage of the fast convergence speed of $l_{2,0}$ mixed norm to improve the speed of calculation and solution. And then, the regularization coefficient in this model can be adjusted adaptively according to the result sparsity of each iteration result under different noise, in which the relatively stable coefficient can be determined only during a few iteration cycles. So the efficiency of the algorithm is improved obviously. Future work includes: Extending the proposed method to achieve high quality InISAR 3D imaging under short CPI; updating the algorithm to apply the maneuvering target in sparse sampling.

Acknowledgments

The authors would like to thank the editors and the anonymous reviewers whose insightful comments have helped to improve the quality of this paper considerably. This work was supported by the Natural Science Foundation of Shandong Province under Grant ZR2021MF025.

References

[1] KANG, B. S., LEE, K., KIM, K. T. Image registration for 3-D interferometric-ISAR imaging through joint-channel phase difference functions. *IEEE Transactions on Aerospace and*

Electronic Systems, 2021, vol. 57, no. 1, p. 22–38. DOI: 10.1109/TAES.2020.3021108

[2] SUWA, K., WAKAYAMA, T., IWAMOTO, M. Three-dimensional target geometry and target motion estimation method using multistatic ISAR movies and its performance. *IEEE Transactions on Geoscience and Remote Sensing,* 2011, vol. 49, no. 6, p. 2361–2373. DOI: 10.1109/TGRS.2010.2095423

[3] OZ, Y., ALP, Y. K., YAZGAN-ERER, I. ISAR imaging under group sparsity constraints using ADMM. In *2020 28th Signal Processing and Communications Applications Conference (SIU).* Gaziantep (Turkey), 2020, p. 1–4. DOI: 10.1109/SIU49456.2020.9302303

[4] KANG, M., LEE, S., KIM, K., et al. Bistatic ISAR imaging and scaling of highly maneuvering target with complex motion via compressive sensing. *IEEE Transactions on Aerospace and Electronic Systems*, 2018, vol. 54, no. 6, p. 2809–2826. DOI: 10.1109/TAES.2018.2830598

[5] XU, G., ZHANG, B. J., CHEN, J. L., et al. Sparse inverse synthetic aperture radar imaging using structured low-rank method. *IEEE Transactions on Geoscience and Remote Sensing*, 2022, vol. 60, p. 1–12. DOI: 10.1109/TGRS.2021.3118083

[6] ZHANG, L., XING, M. D., QIU, C. W., et al. Resolution enhancement for inversed synthetic aperture radar imaging under low SNR via improved compressed sensing. *IEEE Transactions on Geoscience and Remote Sensing*, 2010, vol. 48, no. 10, p. 3824 to 3838. DOI: 10.1109/TGRS.2010.2048575

[7] CANDÈS, E., WAKIN, M., BOYD, S. Enhancing sparsity by reweighted l_1 minimization. *Journal of Fourier Analysis and Applications (Special Issue on Sparsity)*, 2008, vol. 14, no. 5, p. 877–905. DOI: 10.1007/s00041-008-9045-x

[8] FENG, J. J, SUN, Y. N., JI, X. X. High-resolution ISAR imaging based on improved sparse signal recovery algorithm. *Wireless Communications and Mobile Computing*, 2021, p. 1–7. DOI: 10.1155/2021/5541116

[9] CHEN, Q. Q., XU, G., ZHANG, L., et al. Three-dimensional interferometric inverse synthetic aperture radar imaging with limited pulses by exploiting joint sparsity. *IET Radar, Sonar & Navigation*, 2015, vol. 9, no. 6, p. 692–701. DOI: 10.1049/iet-rsn.2014.0275

[10] BI, H., LI, Y., ZHU, D. Y., et al. An improved iterative thresholding algorithm for L_1-norm regularization based sparse SAR imaging. *Science China (Information Sciences),* 2020, vol. 63, no. 11, p. 330–339. DOI: 10.1007/s11432-020-2994-4

[11] LI, Y., JIANG, Z., OSMAN, O. M. O., et al. Mixed norm constrained sparse APA algorithm for satellite and network echo channel estimation. *IEEE Access*, 2018, vol. 6, p. 65901–65908. DOI: 10.1109/ACCESS.2018.2878310

[12] WEI, X., YANG, J., CHEN, W., et al. Translational motion compensation for ISAR imaging based on range joint fast orthogonal matching pursuit algorithm. *IEEE Access*, 2022, vol. 10, p. 37382–37395. DOI: 10.1109/ACCESS.2022.3165020

[13] HONG, T., ZHANG, S., LIU, Y. MTRC compensation for sparse aperture ISAR imaging. In *2020 International Conference on Wireless Communications and Smart Grid (ICWCSG).* Qingdao (China), 2020, p. 52–56. DOI: 10.1109/ICWCSG50807.2020.00020

[14] BABACAN, S. D., MOLINA, R., KATSAGGELOS, A. K. Bayesian compressive sensing using Laplace priors. *IEEE Transactions on Image Processing*, 2010, vol. 19, no. 1, p. 53–63. DOI: 10.1109/TIP.2009.2032894

[15] QIN, D., LIU, D., GAO, X., et al. ISAR resolution enhancement using residual network. In *2019 IEEE 4th International Conference on Signal and Image Processing (ICSIP)*. Wuxi (China), 2019, p. 788–792. DOI: 10.1109/SIPROCESS.2019.8868757

[16] YANG, J., LU, X., DAI, Z., et al. Autofocus method for sparse aperture ISAR based on L0 norm and NLTV regularization. In *2021 IEEE International Geoscience and Remote Sensing Symposium IGARSS.* Brussels (Belgium), 2021, p. 5103–5106. DOI: 10.1109/IGARSS47720.2021.9555148

[17] GU, Y., JIN, J., MEI, S. l_0 norm constraint LMS algorithm for sparse system identification. *IEEE Signal Processing Letters*, 2009, vol. 16, no. 9, p. 774–777. DOI: 10.1109/LSP.2009.2024736

[18] LI, B., LIU, F., ZHOU, C., et al. Fast compressed sensing SAR imaging using stepped frequency waveform. In *2016 IEEE International Conference on Microwave and Millimeter Wave Technology (ICMMT)*. Beijing (China), 2016, p. 521–523. DOI: 10.1109/ICMMT.2016.7761827

[19] XU, Z. B., CHANG, X. Y., XU, F. M., et al. $L_{1/2}$ regularization: A thresholding representation theory and a fast solver. *IEEE Transactions on Neural Networks and Learning Systems*, 2012, vol. 23, no. 7, p. 1013–1027. DOI: 10.1109/TNNLS.2012.2197412

[20] EISEN, M., MOKHTARI, A., RIBEIRO, A. Decentralized quasi-Newton methods. *IEEE Transactions on Signal Processing*, 2017, vol. 65, no. 10, p. 2613–2628. DOI: 10.1109/TSP.2017.2666776

[21] ZHANG, M., WANG, X., CHEN, X., et al. The kernel conjugate gradient algorithms. *IEEE Transactions on Signal Processing*, 2018, vol. 66, no. 16, p. 4377–4387. DOI: 10.1109/TSP.2018.2853109

[22] YE, Q. L., AMINI, A. A., ZHOU, Q. Optimizing regularized Cholesky score for order-based learning of Bayesian networks. *IEEE Transactions on Pattern Analysis and Machine Intelligence*, 2021, vol. 43, no. 10, p. 3555–3572. DOI: 10.1109/TPAMI.2020.2990820

About theAuthors ...

Daiyue SONG was born in 1996. He received his B.S. degree from the Qingdao University, in 2020, where he is currently pursuing the MA.Eng. degree with the College of Electronic Information, Qingdao University. His research interests include radar signal imaging and target recognition.

Qianqian CHEN (corresponding author) was born in 1985. She received her Ph.D. degree in Signal and Information Processing from Xidian University, Xi'an, China, in 2015. She is an Assistant Professor at the Department of Electronic Engineering, Qingdao University. From 2018 to 2019, she was a visiting scholar at the Department of Automatic Control and Systems Engineering, University of Sheffield, UK. Her major research interests are SAR and ISAR imaging.

Kaizhuang LI was born in 1997. He received his B.S. degree from the Qingdao University, in 2020, where he is currently pursuing the MA.Eng. degree with the College of Electronic Information, Qingdao University. His research interests include radar signal sorting and target recognition.